Modeling Magnetic Interactions in High-Valent Trinuclear $[\mathrm{Mn_3^{(IV)}O_4}]^{4+}$ Complexes Through Highly Compressed Multi-Configurational Wave Functions

Giovanni Li Manni*

Department of Electronic Structure Theory, Max Planck Institute for Solid State Research, Heisenbergstraße 1, 70569 Stuttgart, Germany

E-mail: G.LiManni@fkf.mpg.de,giovannilimanni@gmail.com

In this work we apply a quantum chemical framework, recently designed in our laboratories, to rationalize the low-energy electronic spectrum and the magnetic properties of an homo-valent trinuclear $[\mathrm{Mn_3^{(IV)}O_4}]^{4+}$ model of the oxygen-evolving center in photosystem II. The method is based on chemically motivated molecular orbital unitary transformations, and the optimization of spin-adapted many-body wave functions, both for ground- and excited-states, in the transformed MO basis. In this basis, the configuration interaction Hamiltonian matrix of exchange-coupled multi-center clusters is extremely sparse and characterized by a unique block diagonal structure. This property leads to highly compressed wave functions (*oligo-* or *single-reference*) and crucially enables state-specific optimizations. The reduced multi-reference character of the wave function greatly simplifies the interpretation of the ground- and excited-state electronic structures, and provides a route for the direct rationalization of magnetic interactions in these compounds, often considered a challenge in polynuclear transition-metal chemistry.

In this study, strong electron correlation effects have explicitly been described by conventional and stochastic multiconfigurational methodologies, while dynamic correlation effects have been accounted for by multiconfigurational second order perturbation theory, CASPT2. Ab initio results for the $[Mn_3^{(IV)}O_4]^{4+}$ system have been mapped to a three-site Heisenberg model with two magnetic coupling constants. The magnetic coupling constants and the temperature dependence of the effective magnetic moment predicted by the ab initio calculations are in good agreement with the available experimental data, and confirm the antiferromagnetic interaction among the three magnetic centers, while providing a simple and rigorous description of the non-collinearity of the local spins, that characterize most of the low-energy states for this system.

1 Introduction

Key chemical processes, such as the water-splitting reaction and the nitrogen reduction – of potential interest in H_2 and NH_3 industrial production – occur in nature through photo-enzymatic reactions catalyzed by polynuclear transition-metal (PNTM) clusters. Iron-sulfur clusters are involved in the biological reduction of N_2, while the $[Mn_4O_5Ca]$ cluster is responsible for the photo-oxidation of water in the oxygen-evolving center (OEC) of photosystem II (PS-II). These processes are clever examples of the biological utilization of solar energy. Decades of accumulated knowledge have led to a deeper understanding of the structure, formation, and reactivity of these bio-catalysts. However, many questions about the fundamental mechanisms that make these bio-catalysts highly effective remain unsolved, preventing further development in the field of bio-mimetic design.

It is commonly accepted that the catalytic activity of these compounds is bound to the large manifold of low-energy states that characterize their electronic structures. These energetically accessible electronic states allow electronic transitions with ease, and in doing so define the catalytic properties of these compounds. However, precisely these energetically

low-lying electronic states are difficult to resolve and characterize, both at the experimental and theoretical level.

The theoretical characterization of these states by modern quantum chemical methods has been hindered by the computational complexity associated to the description of their ground- and excited-state wave functions.

Density-functional theory in its Kohn-Sham formulation (KS-DFT) has allowed scientists to accurately model chemical processes of unprecedented complexity, its applicability in most cases being limited only by the choice of an approximated exchange-correlation (XC) functional. The development of improved functionals has represented a practical route to circumvent the limits bound to the XC functional approximation. However, when addressing polynuclear transition metal clusters a different weakness of DFT arises.

In conventional KS-DFT the electron density is represented by a single Slater determinant (SD), and the method is often referred to as single-configurational, or more precisely single-determinantal. For low-spin open-shell systems, where unpaired electrons reside on different metal centers, a single SD is not a spin eigenfunction. We refer to the corresponding KS-DFT solutions as broken-symmetry (BS) states. BS states contain no physically meaningful information about spin interactions among the magnetic centers, except perhaps for the extreme collinear solutions, thus in general failing in qualitatively approximating exchange interactions in these systems. This fundamental feature makes the method incompatible with the investigation of the electronic structures of PNTM clusters. Even when they provide correct energetics, BS-DFT methodologies do not provide a qualitatively correct description of the electronic states, and interactions among magnetic centers can easily be misinterpreted. Clear difficulties emerge when interactions among the magnetic centers of PNTM clusters are not *collinear*, that is when local spin-vectors across sites are not parallel (ferromagnetic alignment) or anti-parallel (anti-ferromagnetic alignment).[1] This issue easily arises in PNTM clusters whose magnetic centers have local spin $S_{local} > 1/2$. This is precisely the case of the $[Mn_3^{(IV)}O_4]^{4+}$ system presented in this document.

For a dinuclear system with $S_{local} = 1/2$, only two spin states are possible, with $S_{tot} = 0$ (singlet) and $S_{tot} = 1$ (triplet). Both these cases are collinear, and in general can be described by BS-DFT techniques, upon a suitable choice of exchange-correlation functional. On the contrary, when considering a dinuclear homo-valent system with $S_{local} > 1/2$ the total spin of the low-energy eigenstates will span the range:

$$S^1_{local} + S^2_{local}, \quad S^1_{local} + S^2_{local} - 1, \quad \ldots, \quad 0. \tag{1}$$

While the extreme spin states (the collinear states) can be described by BS-DFT methodologies, the intermediate spin states (the non-collinear states) cannot be described by BS-DFT. As an example, we consider two magnetic centers with $S_1 = S_2 = 3/2$. The total spin can assume values in the range $[3 - 0]$. In BS-DFT a total spin $S_{total} = 1$, can only be obtained by flipping spins in either of the two centers, leading to $S_1 = 1/2$ and $S_2 = 3/2$, or $S_1 = 3/2$ and $S_2 = 1/2$. Obviously these states do not represent physical states; in the best possible scenario they correspond to high-energy non-Hund states, featuring unphysical on-site electron pairing or spin-flips. With more than two magnetic centers of local spin $S_{local} > 1/2$ the inaccuracy in describing non-collinear pair-interactions negatively affects the accuracy in describing competing low-energy states.

Weighted-average BS-DFT methodologies have been employed to mitigate the limitations in the classical KS-DFT.[2,3] In weighted-average methods physical states are approximated by mixing, through diagonalization of effective Hamiltonians, BS states obtained from high-spin states (correctly described by DFT as spins are fully aligned), and other BS states derived from spin-flips at different magnetic centers. While each of the BS states utilized undergo a self-consistent field (SCF) optimization of the orbitals, no SCF procedure is applied to the weighed-averaged states, thus limiting the level of accuracy attainable.

Noncollinear DFT represents an alternative DFT strategy that aims at accurate descriptions of the non-local nature of spin correlations.[4–8] The *extended* BS-DFT represents

another route to cope with the symmetry breaking limitations.[9]

The noncollinear strategy has been applied by Truhlar and coworkers to a $[Mn_3^{(IV)}O_4]^{4+}$ model system, that in the present work are considered for comparison.[7] Only the low-spin ground state (LS), with $S_{total} = 1/2$, and the first excited state (HS), with an $S_{total} = 3/2$, have been discussed in Truhlar's work.[7] This data is sufficient to make a minimal comparison with the work presented here, but not sufficient to obtain simulated magnetic properties, such as extraction of magnetic coupling constants and magnetic susceptibility simulations. In this work the manifold of low-energy states are computed through conventional and stochastic multiconfigurational (MC) procedures, and the extracted magnetic properties are directly compared to the available experimental data.[10]

Ab initio wave function based methods allow for an unbiased evaluation of magnetic interactions in PNTM clusters. However, their broad applicability has been hindered by the exponential scaling of the many-body wave function with respect to the number of correlated electrons. The density matrix renormalization group (DMRG) approach has been widely utilized for circumventing the exponential scaling limitations, and for studying exchange-coupled transition metal clusters.[11–18] Recently also full-CI Quantum Monte-Carlo (FCIQMC),[19–26] and the related Stochastic-CASSCF approach,[27–30] have successfully been applied to TM complexes with one or more metal centers.[27,31–36]

Within wave function based methods, low-spin states consisting of a large number of unpaired electrons, in general exhibit a strong *multi-reference* character, meaning that in the configuration interaction (CI) expansion of the wave function, there are numerous electronic configurations with large relative amplitudes. This property makes their optimization difficult for approximated approaches such as DMRG, FCIQMC and selected-CI strategies. These approximated methodologies partially circumvent the exponential scaling of the Hilbert space with respect to the number of correlated electrons, but typically show slow convergence with respect to the multi-reference character of the wave function.

Very recently, a theoretical strategy has been developed in our laboratories,[34,35] that dras-

tically reduces the multi-reference character in low-spin state wave functions. This strategy is based on MO unitary transformations, consisting of MO localization and reordering, and the expansion of the spin-adapted CI wave function in this transformed MO basis. We have demonstrated that these MO transformations are beneficial to methods that only approximate full-CI wave functions, such as FCIQMC,[19–25,27–30] within the Graphical Unitary Group Approach (GUGA).[26,34,35,37–40] Our protocol has successfully been applied towards the resolution of ground- and excited- states of homo-valent iron-sulfur dimers and cubanes.[34,35] In our earlier work,[34,35] up to 44 electrons have been correlated in a space of 32 orbitals for $[Fe_4S_4]$ cubane systems. This strategy drastically reduced the computational costs associated to the FCIQMC algorithm, thus making large active space calculations routinely feasible. We envision that this strategy will be key for the success of other methodologies that approximate the full-CI wave function, where a CI sub-space is selected and optimized, often referred to as *selected-CI* procedures. There are a number of such procedures; a non-complete list of examples includes Caffarel's Selected-CI approach,[41–44] the iterative-CI procedure by Hoffmann and co-workers,[45,46] and the generalized active space approach,[36,47,48] as long as spin-adaptation is available that relies on cumulative spin coupling of consecutive spins. The *cumulative* spin-adaptation via GUGA has been available within the conventional multiconfigurational methodologies (CAS, RAS) implemented in the (Open)Molcas chemistry software package[28,29] since their early days. Spin adaptation has also been implemented within the generalized active space SCF framework,[47] and very recently made available in Alavi's FCIQMC algorithm.[26]

The interpretation of many-body wave functions and their energetics, once available, represents another important challenge in the application of ab initio quantum chemical methods to PNTM clusters. Crucially, the proposed strategy leads to extremely *compact* many-electron wave functions, of simple and immediate physical interpretation, something that is often difficult to do with other high-level ab initio methods. This aspect represents the main focus of the present work.

All low-energy states with total spin ranging from 1/2 to 9/2, of a $[Mn_3^{(IV)}O_4]^{4+}$ model system have been optimized at the complete active space self-consistent field (CASSCF) level of theory, within the framework of localized and reordered MOs. The MO unitary transformations of the variationally optimized CASSCF wave functions, have allowed us to uniquely characterize the low-energy electronic spectrum of this system. Important dynamic correlation effects not captured by CASSCF have been included by the multiconfigurational second-order perturbation theory (CASPT2) procedure. In order to better understand the correlation effects outside the active space and accounted for at the CASPT2 level of theory, larger active space calculations on selected states have also been performed using FCIQMC.

Having access to the entire low-energy spectrum, magnetic coupling parameters have easily been extracted by mapping the ab initio energies to a three-site Heisenberg–Dirac–van Vleck Hamiltonian[49] with two anti-ferromagnetic coupling constants.

In Section 2, details on the model system and the computational procedures utilized are discussed; a brief introduction on our theoretical strategy is also given. Our ab initio results are summarized in Section 3, and compared to Truhlar's noncollinear results[7] and the available experimental data.[10] The agreement between the calculated and the experimentally measured temperature dependence of the effective magnetic moment,[10] μ_{eff} is of particular relevance. In Section 4 our conclusions are offered.

2 Theoretical and Computational Details

The Model System. Truhlar's model system has been chosen for the present work, to facilitate the comparison of the respective results (Figure 1). In this model the $[Mn_3^{(IV)}O_4]^{4+}$ core system is surrounded by two water molecules and four N,N'-bis(methylene)-Z-1,2-ethenediamine, to mimic the octahedral environment found in the synthetic $[Mn_3O_4(bpy)_4(OH_2)_2]^{4+}$ species.

Both the experimental complex and Truhlar's model system exhibit a low-spin (LS,

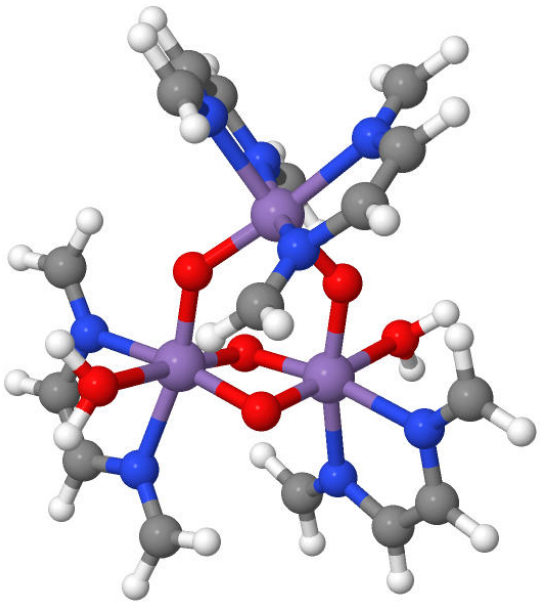

Figure 1: Structure of the $[Mn_3^{(IV)}O_4]^{4+}$ system used in the present work and made available in Reference [7] .

$S_{total} = 1/2$) ground-state, with the first excited state (HS, $S_{total} = 3/2$) at only ~ 65 cm^{-1} above. Experimentally,[10] the LS ground-state has been characterized as a system with local spins $S_A = S_B = S_C = 3/2$, with A and B coupled to spin $S_{AB} = 1$ (non-collinear), further coupled (noncollinear) to the magnetic center C, leading to the $S_{total} = 1/2$ total spin value. On the contrary, in the HS state magnetic centers A and B are anti-ferromagnetically aligned (collinear with $S_{AB} = 0$).

Active Spaces. The three $Mn^{(IV)}$ magnetic centers are characterized by a d^3 electronic configuration. Each magnetic center is surrounded by an octahedral environment created by the external ligands and the bridging oxygen atoms. The five 3 d orbitals are split into the triply-degenerate and singly occupied t_{2g} orbitals, and the empty doubly-degenerate e_g orbitals. Considering the large distance among the Mn atoms in the system ($d_{AB} = 2.68$ Å and $d_{AC} = d_{BC} = 3.27$ Å), ligand-field induced excited states (electron excitations among the t_{2g} and e_g orbitals) are to be considered high-energy states relatively to the low-energy states characterized by the very weak spin interactions across the metal sites of the $[Mn_3^{(IV)}O_4]^{4+}$

model system. Thus, a small active space, that contains only the 9 singly occupied t_{2g} orbitals and their electrons, has been considered as the first inexpensive choice for resolving the low-energy spectrum of the system. We refer to this active space as CAS(9,9). This active space provides a qualitatively correct description of the states of interest, as exchange interactions across the magnetic centers are explicitly considered in the MC wave function for all energetically low-lying spin states. However, this active space is not sufficiently large to account for other forms of correlation, such as the superexchange correlation (involving the bridging atoms), and the above mentioned ligand-field effects (except that in a mean-field manner), which are the two leading forms of many-body electron correlation after spin-exchange interactions. The MC second order perturbation theory, CASPT2, that utilizes the CASSCF(9,9) wave function as reference, has been chosen for accounting these other forms of correlation. It has been demonstrated in one of our earlier works,[31,33] that CASPT2 fails in recovering high-order correlation effects, and the synchronized superexchange excitations among the bridging oxygen atoms and the magnetic centers belong to this form of correlation. Therefore, the CASPT2 results are to be considered cautiously, and only semi-quantitative accuracy is to be expected from the CASSCF(9,9)/CASPT2 protocol. With this limitation in mind, CASPT2 is proven a crucial component in the present work to obtain a qualitatively correct description of correlation effects outside the chosen active space, and sufficient to extract the key magnetic features of the low-energy spectrum for this system. A more reliable procedure to account for the ligand-mediated correlation effects consists in considering these other forms of correlation explicitly, by further enlarging the active space size and solving the exponentially larger CAS wave function via the stochastic FCIQMC algorithm. Thus, a larger active space choice has been made, that allows us to validate the capability of CASPT2 in recovering important correlation effects outside the small CAS(9,9). The converged state-average CASSCF(9,9) natural orbitals for each spin symmetry have been further unitarily transformed, via separate block localization of the inactive and the virtual orbitals – an invariant transformation with respect to the preceding CASSCF(9,9) –. Thus, the 6 metal

centered e_g orbitals, 10 orbitals of the peripheral ligands (orbitals of σ type on the N and O peripheral atoms, pointing directly to the three metal centers and carrying lone-pairs electrons), and the 12 2 p orbitals of the four bridging O atoms have been added to the CAS(9,9). This choice led to the much larger CAS(53,37). The 37 orbitals were sorted by first listing the 10 peripheral σ orbitals, followed by the 12 2 p orbitals of the bridging O atoms, the t_2g orbitals (in site-ordering), that were already considered in the CAS(9,9), and finally the empty e_g orbitals, also site-ordered. Within this active space, the full-CI wave function of the lowest state for each spin symmetry has been optimized via the spin-adapted FCIQMC algorithm. Also, CASPT2 calculations have been performed within the same CAS(53,37) active space, while considering the CASSCF(9,9) wave function as reference, the doubly occupied ligand orbitals as inactive, and the e_g orbitals as virtual orbitals. The remaining orbitals outside the CAS(53,37) were frozen, and not involved in the CASPT2 procedure.

The Wave Function. In this section we discuss in greater details the conceptual framework behind the main features of the wave functions of the low-energy states. Locally the $Mn^{(IV)}$ d^3 centers are formally considered in their high-spin state, $S_A = S_B = S_C = 3/2$, due to Hund's rules. Combining two spin angular momenta with local spin $S_{local} = 3/2$ results in the direct product of the 4 possible intermediate spin states, S_{interm}, namely $\Gamma^{(3/2)} \otimes \Gamma^{(3/2)} = \Gamma^{(3)} \oplus \Gamma^{(2)} \oplus \Gamma^{(1)} \oplus \Gamma^{(0)}$. The resulting intermediate spins, S_{interm}, further couple to the third local spin, $S_{local} = 3/2$, producing the spin states reported in Equation 2.

$$
\begin{array}{lccccccccc}
\Gamma^{(3)} \otimes \Gamma^{(3/2)} = & \Gamma^{(9/2)} & \oplus & \Gamma^{(7/2)} & \oplus & \Gamma^{(5/2)} & \oplus & \Gamma^{(3/2)} & & - \\
\Gamma^{(2)} \otimes \Gamma^{(3/2)} = & - & & \Gamma^{(7/2)} & \oplus & \Gamma^{(5/2)} & \oplus & \Gamma^{(3/2)} & \oplus & \Gamma^{(1/2)} \\
\Gamma^{(1)} \otimes \Gamma^{(3/2)} = & - & & - & & \Gamma^{(5/2)} & \oplus & \Gamma^{(3/2)} & \oplus & \Gamma^{(1/2)} \\
\Gamma^{(0)} \otimes \Gamma^{(3/2)} = & - & & - & & - & & \Gamma^{(3/2)} & - &
\end{array}
\tag{2}
$$

Thus, a total of 12 low-energy spin states are generated by the coupling of three $S_{local} =$

3/2 spin angular momenta, spanning total spin values from $S_{total} = 9/2$ to $S_{total} = 1/2$. For $S_{interm} = 3$, the spins on the first two centers are parallel (collinear). The third center can couple to the previous two in a collinear manner, leading to $S_{total} = 9/2$ (trivial wave function with all spin parallel aligned), and $S_{total} = 3/2$, with the spin on the third center anti-parallel with respect to the intermediate subsystem (AB). Analogously, for $S_{interm} = 0$ the first two centers show anti-parallel spins (collinear), while the third center is left uncoupled. The remaining 9 spin states are characterized by non-collinear spin-couplings, including the LS state.

Within the ab initio methodologies the difficulty of representing non-collinear states is circumvented, as the necessary degrees of freedom for the spin couplings are accounted for by the components of the MC wave functions (CSFs are to be considered a complete set of versors in the CI Hilbert space). How the spin couplings are represented in the many-body wave function, however, depends on the one- and many-particle representation. When MOs are delocalized over the magnetic centers the interaction among local spins is described at the price of an highly multi-reference wave function. In the delocalized MO basis no leading configurations can promptly be identified, and even upon optimization of the wave function its interpretation is rather cumbersome.

Localization of the MOs leads to more compact wave functions. This feature arises from the fact that localized orbitals represent well the *locality* of spins. Within this one-electron basis, however, if Slater determinants are used as many-particle basis the MC wave function will still be characterized by a strong multi-reference character. We can relate this property to the description of the H_2 molecule at dissociation through atomic orbitals ($1\,s_A$ and $1\,s_B$), instead of the symmetry adapted σ_g and σ_u^* molecular orbitals. In the former basis, the ground state wave function is single-configurational in the spin-adapted basis of configuration state functions (CSFs), $|1s_A^u 1s_B^d\rangle$ (u and d superscripts refer to the up- and down- spin couplings), while two Slater determinants are required to correctly describe the same state, $|(1s_A^\alpha 1s_B^\beta - 1s_A^\beta 1s_B^\alpha)\rangle$. On the contrary, in the symmetry adapted MO representation, the

ground state wave function is a perfect mixing of two electronic configurations, $|\sigma_{\mathrm{g}}^2\rangle$ and $|\sigma_{\mathrm{u}}^2\rangle$.

The number of *leading* CSFs – i.e. the number of spin adapted electronic configurations with large CI amplitudes relatively to the entire CI vector – in the localized basis can be estimated by the van Vleck-Sherman formula:[50]

$$g(n_o, S) = \binom{n_o}{n_o/2 - S} - \binom{n_o}{n_o/2 - S - 1}. \tag{3}$$

where n_o and S refer to the number of singly occupied orbitals and the total spin, respectively. In this basis the reference space consists, in general, of all possible distributions of spins among the singly occupied orbitals, thus defining a system of interacting spins (*spin-system*).

Further compression can be achieved if the localized orbitals are *site-ordered*, meaning that first we list all orbitals of magnetic center A, then we list all orbitals of the center B and so on. By this ordering the unpaired electrons directly relate to the local spin angular momentum within each magnetic center; they are not to be considered individually but in groups, each group consisting of cumulatively coupled spins to match the local spin on the fragments A, AB, ABC, and so on. This concept applies well as long as non-Hund configurations are energetically well separated from the atomic ground-states (even upon considering ligand field effects) and thus play a marginal role, which is to be expected for most – if not all – low-energy states of high-valent polynuclear transition metal clusters. This property is best described graphically by means of the genealogical branching diagrams, as described in the following.

In Figure 2a, we show a general genealogical branching diagram, in which all leading configuration state functions spanned by the MC wave function can be identified as paths branching through the diagram. Genealogical branching diagrams only describe spin couplings among unpaired electrons. Configurations with electron pairing, arising from charge transfer excitations or local pairing are not represented by these diagrams. This feature makes these diagrams extremely powerful in describing the leading configurations in systems

mostly dominated by spin-exchange interactions. The *node weights* (number inside each node) represent the number of paths (thus CSFs) for a given number of unpaired electrons, N_e, coupled to a specific spin, S. The node weight can be derived from the van Vleck-Sherman formula, or graphically by summing the node weights of the nodes connected from the left.

In the localized and site-ordered basis some paths in the branching diagram can trivially be recognized as deadwood configurations. These are the ones that describe non-Hund configurations, and have been marked in gray in Figure 2b and Figure 2c.

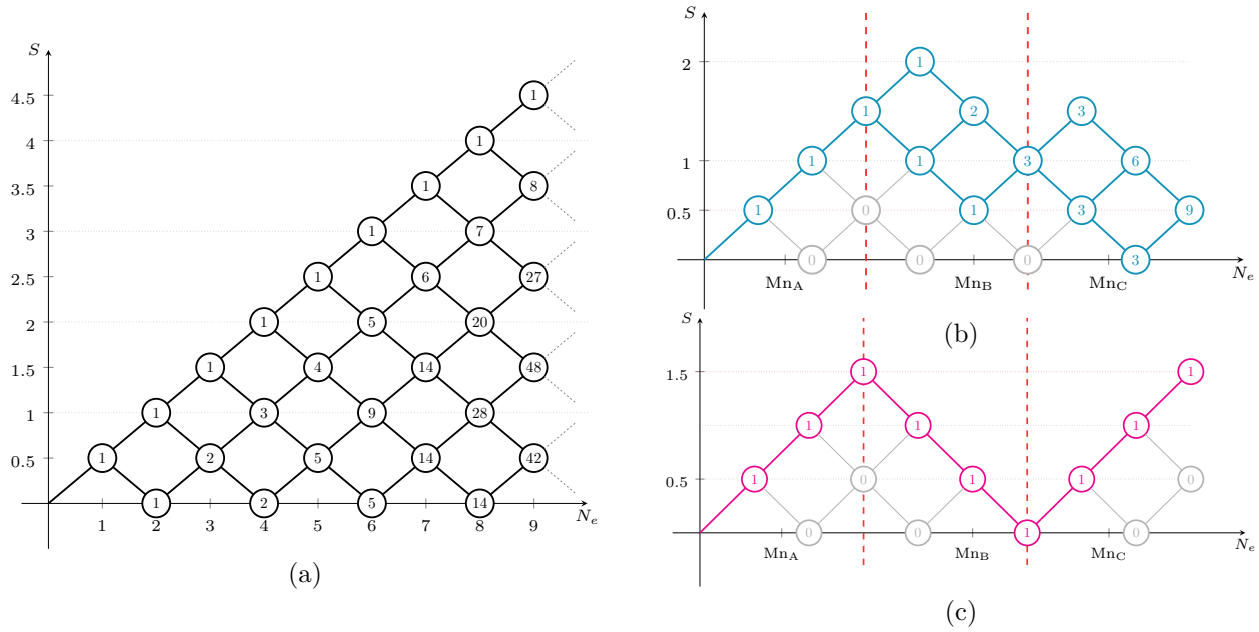

Figure 2: Left: Generic genealogical branching diagram for up to 9 electrons (N_e). The node weights represent the number of paths starting from the root node, $(N_e, S_{tot}) = (0, 0)$ to reach the targeted node. This number is given by the van Vleck-Sherman formula, Equation 3. Top right: in light blue the paths corresponding to the 9 leading CSFs of the $S_{tot} = 1/2$ LS state. Bottom right: in purple the single path that corresponds to the single-reference HS state. The gray paths correspond to non-Hund CSFs that become deadwoods in the localized and site-ordered MO basis.

The nodes of these *deadwood* configurations have their weights suppressed (set to zero), thus leading to an overall reduction of the number of leading configurations for a given target state, even with respect to the already reduced size given by Equation 3.

In Figures 2b and 2c only the significant paths leading to the LS and the HS states (proposed by experiments) have been highlighted. Figure 2c shows the local spin $S_A = 3/2$

of the first magnetic center, the anti-ferromagnetic spin alignment of Mn_B with respect to Mn_A, ($S_{AB} = 0$), and the last three electrons on Mn_C with their spin aligned ($S_{total} = 3/2$). The negligible non-Hund configurations become apparent in this diagram (marked in gray). The single magenta path of Figure 2c indicates that a MC wave function, optimized for this state in the localized and site-ordered MO basis, is inherently single-reference (to the leading terms). The unique single-reference character of this wave function is to be compared to the highly dense wave functions obtained in other MO representations of the same state. As shown in Figure 2a, this state would contain 48 leading configurations if represented in localized and non-site-ordered basis, and thousands of CSFs with comparable amplitudes in the delocalized basis (more details in Section 3).

In Figure 2b parallel spins are promptly recognized for the Mn_A site ($S_A = 3/2$). Mn_B is coupled to Mn_A leading to $S_{AB} = 1$. This intermediate state can be reached via three different paths. The coupling of Mn_C, leading to the final $S_{total} = 1/2$ spin, arises via three more paths. Thus, 9 CSFs are to be expected to be the leading terms of the CI expansion for this state; a substantial simplification with respect to the 42 configurations in a localized and non-reordered MO basis (as shown by Figure 2a), and a even larger compression with respect to the expansion in delocalized basis.

The identification of vanishing paths is only possible in the site-ordered MO basis, as consecutive spins (located on the same site) are directly coupled one to the other in a cumulative way. If electrons located to the same magnetic site are not contiguous (for an unfortunate choice of orbital ordering) their spin coupling will be mediated by the interposed spins. This can only be done at the price of a more dense (multi-reference) wave function.

When maximal compression is reached (to the limit of single configurational wave functions) interpretation of spin interaction becomes trivial, as it will be shown in Section 3.

This conceptual framework combines well with the stochastic optimization of wave functions within FCIQMC. In FCIQMC, in its CAS form, no constraints are imposed to the wave function optimization. At convergence, the leading configurations will generally correspond

to the possible paths of the genealogical branching diagrams. If deviations from the spin-system character exist for the system under investigation, these are promptly recognized. For example, if strong ligand field effects are present, non-Hund contributions may increase, and non-Hund configurations may populate the optimized wave function.

Additional Computational Details. Generally-contracted atomic natural orbitals (ANO-RCC) basis sets[51,52] have been utilized for all computations, obtained from the Mn (21s, 15p, 10d, 6f, 4g, 2h), C, N, O (14s, 9p, 4d, 3f, 2g), and H (8s, 4p, 3d, 1f) primitive functions. Basis set dependence of the correlated calculations has been tested by employing two contraction schemes. In one case the primitive functions have been contracted to Mn(5S4P2D), O(3S2P), C,N(2S1P), H(1S), giving a basis set of double-ζ quality (VDZ). In a larger basis set (labeled VTZ) the primitive functions have been contracted to Mn(6S5P3D2F1G), O(4S3P2D1F), C,N(3S2P), H(2S), giving a basis set of split-valence triple-ζ plus polarization quality for the core cluster, and bridging O atoms, and of double-ζ quality for the peripheral groups. This second basis set choice led to a total of 629 basis functions. Scalar relativistic effects were introduced via second order Douglas-Kroll-Hess integral correction. The evaluation of the electron repulsion integrals has been greatly simplified by means of the resolution-of-identity Cholesky decomposition technique,[28,29] with a decomposition threshold of 10^{-4} a.u.[53–57]

Orbitals have been localized using the Pipek-Mezey localization scheme,[58] thus, the point group symmetry of the molecule was not enforced in our computations. State-Averaged (SA) CASSCF(9,9) calculations were performed separately for each spin sector. Within the OpenMolcas chemistry software package,[29] utilized for the present investigation, it is not possible to perform SA calculations across multiple spin-states. Thus, it has not been possible to address the question of whether performing a global SA calculation over all 12 states, could possibly have some effects in the results and in their interpretation.

For the CASPT2(9,9) calculations the lowest 45 core orbitals have been kept frozen, consisting of the $1s$ orbitals on C, N and O atoms, and $1s2s2p$ shells on the Mn centers.

The default IPEA shift value of 0.25 a.u. has been utilized for the CASPT2 calculations used in extracting the magnetic spin constants. However, for probing the stability of the method a number of IPEA shift values (0.4, 0.3, 0.25, 0.2 and 0.1) have been utilized for the CASPT2(9,9)//(53,37). For the stochastic-CAS(53,37) calculations up to 10^8 walkers have been utilized. All spin-adapted FCIQMC dynamics have been performed using the NECI code.[30]

3 Results

Structure of the CAS(9,9) wave functions. In this section the wave functions of the two lowest spin states are discussed, namely the LS ground state, with $|\mathrm{S_{AB}}, \mathrm{S_{total}}\rangle = |1, 1/2\rangle$, and the HS state, with $|\mathrm{S_{AB}}, \mathrm{S_{total}}\rangle = |0, 3/2\rangle$, as well as the excited states within the same spin sectors. Two low-energy doublets and four quartet states have been computed at the state-average (SA) CASSCF/PT2(9,9) level of theory, corresponding to the doublet and quartet states summarized in Equation 2. The leading configurations of the optimized CASSCF(9,9) wave functions for these states are summarized in Table 1. For the LS ground state 9 leading configurations are identified, while for the HS state the wave function is dominantly single-reference within the localized and site-ordered MO basis, and the GUGA genealogical spin-coupling scheme. Most interestingly, within the localized and site-ordered MO basis, the leading terms of the optimized wave functions of the LS and the HS states, correspond to the highlighted paths reported in Figure 2b and Figure 2c, that we can predict by theoretical arguments based on simple rules of the spin couplings.

All leading CSFs, independently of the targeted spin state, are characterized by a local $S_\mathrm{A} = 3/2$ spin value, indicating that no mixing with non-Hund states has occurred, and that non-Hund states are energetically well separated from the low-energy states. Moreover, for the LS state an intermediate $S_\mathrm{AB} = 1$ spin value is promptly identified from inspection of the leading CSFs, while the HS state is characterized by an intermediate $S_\mathrm{AB} = 0$ spin

value. These results confirm the experimental data[10] and provide additional details on the electronic structures, complementary to Truhlar's non-collinear approach.[7]

In Figure 3 we report the weights of the CASSCF(9,9) wave function for the LS state, $|S_{AB}, S_{total}\rangle = |1, 1/2\rangle$, in three different MO representations, namely, the delocalized natural orbitals, the localized orbitals with an arbitrary MO ordering, and the localized and site-ordered orbitals. The multi-reference character of the $|1, 1/2\rangle$ state in the delocalized natural

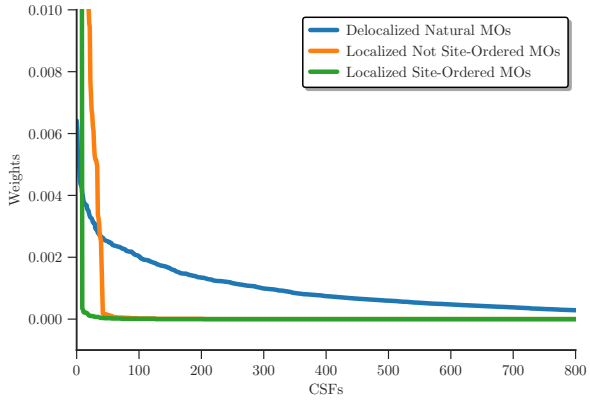

Figure 3: Weights in decreasing order of the CASSCF(9,9) wave function of the $|1, 1/2\rangle$ state in three different MO basis: delocalized natural orbitals (blue), localized non-site-ordered orbitals (yellow) and localized and site-ordered orbitals.

orbital basis (blue curve in Figure 3) is demonstrated by the very slowly decreasing of the CI weights; 1332 CSFs out of the 8820 CSFs of the entire configurational space have weights larger than 10^{-4}. The wave function is more compact within the two localized basis. However, in the localized basis without site-ordering (yellow curve) 42 elements with weights larger than 10^{-4} can be identified. Not surprising, this number corresponds to the node weight in Figure 2a for a system with 9 unpaired electrons and $S_{total} = 1/2$. On the contrary, in the localized and site-ordered MO basis (green curve) there are only 9 leading CSFs, corresponding to the ones shown in Figure 2b and Table 1. The level of compression is substantial. This represents a numerical proof that in the site ordering non-Hund CSFs become *deadwood* configurations and a natural compression of the wave function is obtained. Moreover, in the site-ordered basis the structure of these wave functions directly provide information on the intermediate spin couplings, as shown in Table 1, information that is not

available in other orbital representations. Similar observations apply to all other spin states in their ground- or excited-states.

Relative energies. This section focuses on the CASSCF and CASPT2 relative energies of the 12 low-energy states of the Mn_3O_4 model system. While the CASSCF(9,9) wave functions have correct spin coupling structures, an incorrect energy ordering of states is obtained at this level of theory. Within each symmetry sector, states with higher $S_{\rm AB}$ values are predicted at lower energy than states with a lower $S_{\rm AB}$ value. For example, the $|S_{\rm AB}, S_{\rm tot}\rangle = |3, 3/2\rangle$ state is predicted at lower energy than the $|S_{\rm AB}, S_{\rm tot}\rangle = |0, 3/2\rangle$ state. Similarly, the $|2, 1/2\rangle$ state is predicted the lowest doublet state by CASSCF(9,9), with the $|1, 1/2\rangle$ at 69 $\rm cm^{-1}$ above. The higher spin states are over-stabilized with respect to the low-spin states, and the $S_{\rm tot} = 9/2$ is erroneously predicted to be the ground state.

CASPT2(9,9) corrects the energy ordering of the states. The CASPT2 correction is large and qualitative in character. The lowest doublet state corresponds to the $|1, 1/2\rangle$ state, with the $|2, 1/2\rangle$ state at 158 $\rm cm^{-1}$ above, in qualitative agreement with the experimental predictions.[10] Moreover, higher spin states are predicted at higher energy by CASPT2.

This result represents a strong indication that the small CASSCF(9,9) does not contain the important correlation mechanisms, which are recovered by the subsequent CASPT2 correction. Important correlation effects exist, which are outside the CAS(9,9) wave function, that are responsible for the correct ordering of states; the superexchange mechanism, which involves the bridging oxygen atoms, and ligand field effects (both arising from correlation bound to the peripheral ligands, and the ligand field splitting between the t_{2g} and the e_g orbitals), are certainly the most important of these effects. The superexchange mechanism across the di-μ-oxo bridge is to be expected to play a crucial role in stabilizing the low intermediate and total spin-states over the high spin couplings.

Larger active spaces, CAS(53,37). The role of the charge-transfer excitations, involving the bridging O atoms and the peripheral ligands, and of the $d - d$ excitations between the

t_{2g} and the e_g orbitals has been investigated by the larger CAS(53,37), where the above mentioned orbitals and their electrons have explicitly been correlated. Due to the size of this active space, prohibitive for conventional CAS eigensolvers, the FCIQMC algorithm has been chosen to optimize the lowest state for each spin symmetry. For comparison, also a CASPT2(9,9)/(53,37) calculation has been performed, that is a conventional CASPT2 calculation that uses the CASSCF(9,9) wave function as reference, and in which any orbital outside the CAS(53,37) space has been frozen and not included in the PT2 excitations for generating the perturber space.

The Stochastic-CAS(53,37) wave function of the lowest state of each spin symmetry has been selectively optimized by choosing the highest weighted CSF of the CAS(9,9) as reference for the FCIQMC dynamics. For example, the (uuudduddu) CSF has been chosen as reference for the LS ground state, as shown in Table 1. In the (uuudduddu) nomenclature the occupancy of the doubly occupied peripheral and bridging orbitals, and the empty e_g orbitals of the CAS(53,37) are implied. The highest weights of the optimized LS and HS wave functions are reported in parenthesis in Table 1, next to the corresponding weights of the smaller CAS(9,9). The relative weights of the leading CSFs of the CAS(53,37) reflect the ordering obtained for the CAS(9,9), albeit all weights appear substantially reduced. This reduction follows directly from the fact that in the large CAS(53,37) important excitations exist outside the 9 formally singly occupied orbitals. In the CAS(9,9), after the leading CSFs reported in Table 1, CSFs with low weights ($\sim 0.02\%$) are found, that represent metal-to-metal charge-transfer excitations. On the contrary, in the CAS(53,37) numerous CSFs with weights of $\sim 0.1\%$ are found, that correspond to single excitations from the bridging O to the t_{2g} orbitals. These configurations describe explicitly the superexchange mechanism, whose excitations are absent in the CAS(9,9). Also, single and double excitations from the bridging O atoms to the empty e_g orbitals can be identified. This latter class of excitations are a clear reminder of how ligand field effect is a form of many-body electron correlation. Direct metal-to-metal charge transfer excitations exist also for the CAS(53,37) wave function, and

similarly to the CAS(9,9) their weights are relatively low $\leq 0.02\%$. Excitations from the peripheral ligands to the metal centered orbitals are also low-weighted ($\leq 0.01\%$).

Figure 4 shows the relative energy of the spin-ladder from $S_{\text{tot}} = 1/2$ to $S_{\text{tot}} = 9/2$.

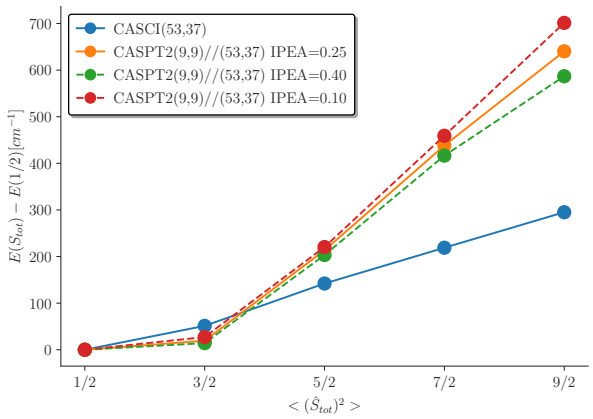

Figure 4: Relative energy [cm^{-1}] of the spin-ladder for the $Mn_3^{(IV)}O_4$ model system at the CAS-CI(53,37) and CASPT2(9,9)//(53,37) level of theory. For the CASPT2 energies the default IPEA shift value of 0.25 a.u. has been utilized (solid yellow curve) along with a lower (0.1 a.u., dashed red curve) and a higher (0.4 a.u., dashed green curve) values.

The CASCI(53,37) and the CASPT2(9,9)//(53,37) span an identical correlation space. It is therefore surprising to observe the quantitative discrepancy reported in Figure 4. At the CASPT2 level, a number of parameters might be responsible for the deviations from the optimal spin-ladder energies. We have probed the dependency on the IPEA shift value and found that larger and smaller IPEA shift values increase and decrease the lowest-to-highest spin-gap, respectively, by ~ 100 cm^{-1}, which is not sufficiently large to justify the difference of about 350 cm^{-1} between the CASPT2 and the FCIQMC highest spin-state energies. Even more surprising is that the discrepancy is such that the CASPT2 lowest-to-highest spin-gap is substantially larger than the FCIQMC values. In fact, it is well known that CASPT2 generally over-stabilizes high-spin states over lower-spin states; the Fe(II)-porphyrin case studied in Reference [31] is an example of the high-spin over-stabilization by CASPT2. However, in the present case the low-spin state is over-stabilized by CASPT2 when compared to FCIQMC predictions. The rationale behind this quantitative discrepancy remains an open question.

Independently of the quantitative considerations, both approaches indicate a doublet ground state, with increased energies for higher spin states. The qualitatively correct CAS(53,37) results are to be directly compared to the incorrect spin ordering obtained at the CASSCF(9,9) level of theory, for which an inverted spin-ladder ordering is observed, with the highest spin-state ($S_{\rm tot} = 9/2$) as ground state. This result numerically demonstrates the important difference between the small CAS(9,9), that describe solely direct spin-exchange interactions, and the much larger CAS(53,37), where ligand mediated correlation effects are explicitly considered in the multi-configurational wave function. In our previous work on Fe_4S_4 cubanes a similar behavior was observed, when comparing the CAS(20,20) to the CAS(44,32). However, in that case the effect was mainly a quantitative effect. In fact, already the CAS(20,20) showed the correct ordering of the six singlet spin-states investigated.

Model Hamiltonian. The CASSCF(9,9)/PT2 states have been mapped to a three-site Heisenberg model with two magnetic coupling constants

$$\hat{\mathcal{H}}_{\rm mod} = J_{2\mu}\left(\mathbf{S}_A \cdot \mathbf{S}_B\right) + J_{1\mu}\left(\mathbf{S}_A \cdot \mathbf{S}_C + \mathbf{S}_B \cdot \mathbf{S}_C\right), \tag{4}$$

where $J_{2\mu}$ and $J_{1\mu}$ are the two non-equivalent coupling constants, one representing the magnetic interaction across the di-μ-oxo bridge ($J_{2\mu} = J_{\rm AB}$) and one the magnetic interactions across the mono-μ-oxo bridges ($J_{1\mu} = J_{\rm AC} = J_{\rm BC}$). The model Hamiltonian has been simplified by considering equivalent $\mathrm{Mn_A - Mn_C}$ and $\mathrm{Mn_B - Mn_C}$ magnetic interactions, thus assuming $\mathrm{J_{AC} = J_{BC}}$. The analytical expression for the eigenvalues can be obtained following the vector model suggested by Kambe.[59] We consider:

$$S_{\rm A} = S_{\rm B} = S_{\rm C} = S_{\rm loc}, \tag{5}$$

$$\mathbf{S}_{\rm AB} = \mathbf{S}_{\rm A} + \mathbf{S}_{\rm B}, \tag{6}$$

$$S_{\rm AB}(S_{\rm AB}+1) = 2\mathbf{S}_{\rm A} \cdot \mathbf{S}_{\rm B} + 2S_{\rm loc}(S_{\rm loc}+1), \tag{7}$$

$$S_{\rm tot}(S_{\rm tot}+1) = \\ 2\mathbf{S}_{\rm A}\cdot\mathbf{S}_{\rm B} + 2\mathbf{S}_{\rm A}\cdot\mathbf{S}_{\rm C} + 2\mathbf{S}_{\rm B}\cdot\mathbf{S}_{\rm C} + 3S_{\rm loc}(S_{\rm loc}+1). \tag{8}$$

Replacing Equation 7 and 8 in Equation 4 directly leads to the eigenvalue equation:

$$\begin{aligned} E(S_{\rm loc},&S_{\rm AB},S_{\rm tot}) = \\ &\frac{J_{2\mu}}{2}\left[S_{AB}(S_{AB}+1) - 2S_{\rm loc}(S_{\rm loc}+1)\right] + \\ &\frac{J_{1\mu}}{2}\left[S_{\rm tot}(S_{\rm tot}+1) - S_{\rm AB}(S_{\rm AB}+1) - S_{\rm loc}(S_{\rm loc}+1)\right]. \end{aligned} \tag{9}$$

This equation applies whenever eigenstates of the total spin are also eigensolutions of the intermediate spin, $\mathbf{S}_{AB}$, and as discussed in the previous section, the wave functions of all low-energy states of the model system satisfy this condition.

We have evaluated the exchange coupling parameters by fitting the eigenvalues of the model Hamiltonian to the corresponding CASPT2 energies. The values obtained, $J_{2\mu} = 152.3$ cm^{-1} and $J_{1\mu} = 92.1$ cm^{-1}, are in good agreement with the ones derived experimentally ($J_{2\mu} = 182$ cm^{-1} and $J_{1\mu} = 98$ cm^{-1}), and clearly indicate anti-ferromagnetic coupling for both pair-interactions, with the coupling between the two Mn centers interacting via the di-μ-oxo bridges (AB) substantially stronger than the coupling between the metal centers connected via the mono-μ-oxo bridges. This result reflects the geometry of the system, with the $\rm Mn_A{-}Mn_B$ bond distance (2.68 Å) shorter than the $\rm Mn_A{-}Mn_C$ and the $\rm Mn_B{-}Mn_C$ atomic distances (3.27 Å).

The energy splittings of the 12 states obtained from Equation 9 and using the ab initio magnetic coupling constants are shown in Figure 5, along with the ones derived experimentally and mapped to the same model Hamiltonian.

The spin gap between the LS and the HS states is 85 cm^{-1} for the TZ basis set (78 cm^{-1} for the DZ basis set), in very good agreement with the magnetic constants obtained from experiments (63.0 cm^{-1}) and suggested by Truhlar's noncollinear approach[7] ($\sim$ 70 cm^{-1}, in Reference [7] reported as 0.2 kcal/mol). The fitted magnetic coupling constants and the

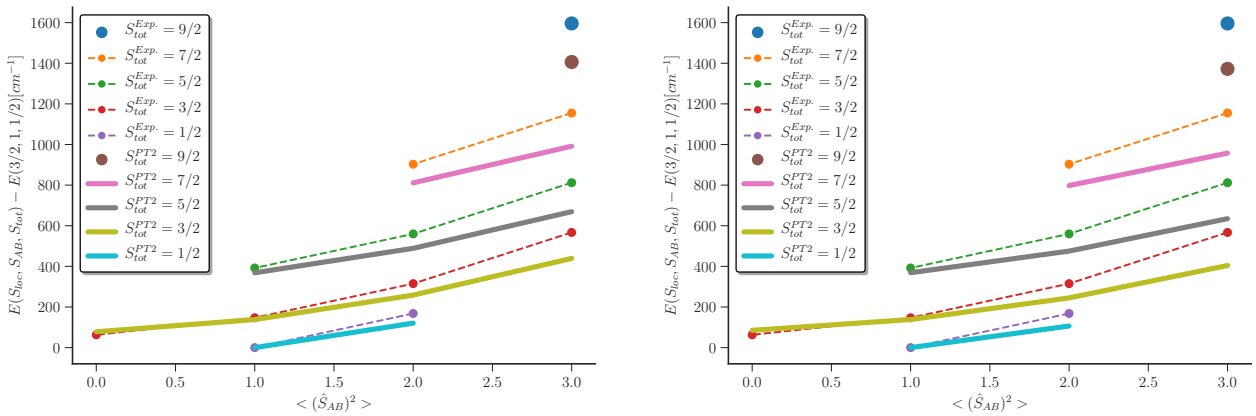

(a) (b)

Figure 5: Energies [cm^{-1}] of the 12 low-energy states of the model system here investigated, relative to the LS ground state, $|S_{\text{loc}}, S_{\text{AB}}, S_{\text{tot}}\rangle = |3/2, 1, 1/2\rangle$, obtained from Equation 9, and using the experimental[10] (dashed lines) and the ab initio (solid lines) magnetic coupling constants. (a) uses the DZ basis CASPT2 energetics, while (b) uses the TZ basis CASPT2 energetics for the mapping. The individual curves identify one specific total spin sector, while the intermediate spin coupling (S_{AB}) is given by the x-axis.

energy ordering of states, summarized in Figure 5 show that the basis set plays a marginal role in describing the magnetic interactions in this model system, despite the basis set has been substantially enlarged, with a total of 283 and 629 basis functions for the DZ and the TZ basis set, respectively.

When compared to experiments, the ab initio relative energies of the higher spin states are partially under-estimated. The largest deviation occurs for the highest spin state, $S_{\text{total}} = 9/2$. Experimentally this state is at 1596 cm^{-1} above the LS ground state, while it is only 1372 cm^{-1} above for the ab initio counterpart within the TZ basis set (1406 cm^{-1} for the DZ basis set).

Within a given spin sector (states lying on the same curve in Figure 5), energy splittings are directly proportional to the $(J_{2\mu} - J_{1\mu})$ difference, and for $J_{2\mu} > J_{1\mu}$, states with lower intermediate spin S_{AB} are more stable than states with higher S_{AB}. Energy splittings among states with same S_{AB} value and varying in total spin (states on the same vertical line of Figure 5), are directly proportional to the $J_{1\mu}$ value. Larger $J_{1\mu}$ values would increase the gaps between these states. The ab initio spin gaps among states with same S_{AB} and different

S_{tot}, are in good agreement with the experimental data available. Thus, the deviations of our results from the experimental values can mostly be ascribed to the fact that the $J_{2\mu}$ value has been partially underestimated relatively to $J_{1\mu}$. In turn, this can be related to the fact that higher-order excitations with respect to the reference CAS wave function are not described by CASPT2.

The finding that spin gaps within the same total spin sector are under-estimated, while spin-gaps within the same S_{AB} sector are well represented, suggests that the underlying reason for this deviations are not to be related to the state-averaging procedure across multiple spin states, but rather to a quantitatively incorrect description of correlation energy for the excited states with respect to the ground state within the same total spin sector.

Paramagnetic Susceptibility. The dependency of the magnetization, M, of a material in an homogeneous external magnetic field, with respect to the strength of the magnetic field, H, known as the *magnetic susceptibility*, χ,

$$\chi = \frac{\partial M}{\partial H}, \tag{10}$$

depends on the magnetic properties of the material, at the microscopic level.[49]

The connection of the magnetic susceptibility to the low-energy states can be described by the van Vleck formula for the Susceptibility (Equation 11).[49,60] In Equation 11, N_{A} is

$$\chi = \frac{N_{\mathrm{A}}\mu_0\mu_B^2 g^2}{3kT} \frac{\sum_{S_{\mathrm{AB}}=0}^{2S_{\mathrm{A}}} \sum_{S_{\mathrm{tot}}=|S_{\mathrm{AB}}-S_{\mathrm{B}}|}^{S_{\mathrm{AB}}+S_{\mathrm{B}}} S(S+1)(2S+1)\exp\left(-E[S,S_{\mathrm{AB}}]/kT\right)}{\sum_{S_{\mathrm{AB}}=0}^{2S_{\mathrm{A}}} \sum_{S_{\mathrm{tot}}=|S_{\mathrm{AB}}-S_{\mathrm{B}}|}^{S_{\mathrm{AB}}+S_{\mathrm{B}}} (2S+1)\exp\left(-E[S,S_{\mathrm{AB}}]/kT\right)}, \tag{11}$$

Avogadro's number, μ_0 and μ_{B} are the vacuum permeability and the Bohr magneton constants, respectively, k refers to Boltzmann's constant (0.695034800 $\mathrm{cm}^{-1}/\mathrm{K}$), and T refers to the absolute temperature. A g = 1.97 value has been chosen, to reflect the one experimen-

tally determined.[10] With the eigenvalues of the low-energy states available, this equation describes the magnetic susceptibility temperature dependence. Equation 11 is related to the *effective magnetic moment*, μ_{eff}, by the following equation:[61]

$$\mu_{\text{eff}} = (\frac{3kT}{N_A \mu_0 \mu_B^2}\chi)^{1/2}. \tag{12}$$

In Figure 6 we compare the temperature dependence of the experimental[10] and the ab initio effective magnetic moments.

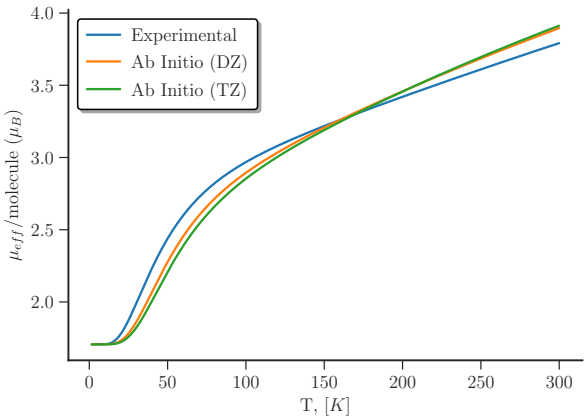

Figure 6: The ab initio temperature dependence of the effective magnetic moment, μ_{eff}, compared to the the one observed experimentally.

The agreement between the effective magnetic moment experimentally measured and the one computed in this work is generally good, despite the quantitative limitations of the CASPT2 methodology discussed above. The discrepancy between the DZ and TZ basis set results is small.

4 Conclusions and Final remarks

In this work, an efficient procedure has been presented, based on MO unitary transformations (localizations of the singly occupied MOs and their site-reordering) and the cumulative spin coupling of adjacent spins, here obtained via the GUGA approach. This strategy provides

extremely compact many-body wave functions for the low-energy states of exchange-coupled homo-valent systems, such as the $Mn(IV)_3O_4$ system investigated in this work. Within this strategy optimized multi-configurational wave functions are obtained that show a limited number of configurations with relatively large CI coefficients (*oligo-reference* wave functions), to the limit of being *single-reference*, such as the wave function of the HS state. The locality of the spins has been known for decades in the inorganic chemistry community, starting from the pioneering work of Anderson and Hasegawa[62] Mouesca and Noodleman[63] and Girerd.[64] Our strategy allows us to take advantage of spin locality in the context of many-body wave function representations, and allows non-Hund configurations to become deadwood configurations (configurations with vanishingly small CI coefficients). This strategy has been proven extremely beneficial in the application of the spin-adapted FCIQMC algorithm, as demonstrated by the present study and our earlier works on Fe_2S_2 and Fe_4S_4 model systems.[34,35] We expect that similar effects are to be observed in other selected-CI approaches, as long as a cumulative spin coupling scheme is employed, for example via GUGA.

Three crucial features emerge from the proposed strategy: (1) an extreme compression of ground- and excited-state wave functions, (2) an unprecedented (quasi-) block-diagonal structure of the CI Hamiltonian, that allows state-specific optimizations, and (3) a simple characterization of the targeted states. These properties make of the proposed approach a powerful tool in electronic structure theory, to understand spin interactions in PNTM clusters and extract magnetic properties of practical interest.

In this work, through the investigation of the low-energy states of the $Mn(IV)_3O_4$ system (spin-ladder), the applicability of our strategy is extended to states with total spin $S_{\text{tot}} \neq 0$, and for systems whose valence orbitals (the 3 d orbitals in the present case) are not necessarily half-filled. These results are very promising and suggest the generality of the proposed strategy, and its potential application to homo- and ethero-nuclear mixed-valence systems. This topic will be discussed in greater detail in a separate work.

Our strategy makes large CAS calculations on ground- and excited-states of PNTM

clusters computationally inexpensive, and the associated magnetic properties of easy interpretation, two aspects to date considered very challenging.

In the localized and site-ordered basis the noncollinear nature of the spin interactions within the three magnetic sites of the $[Mn_3^{(IV)}O_4]^{4+}$ model system is promptly obtained, with the doublet LS ground state featuring an intermediate $S_{AB} = 1$ spin coupling, in agreement with the experimental results. Additionally, an anti-parallel spin alignment (perfectly collinear), $S_{AB} = 0$, is predicted for the first excited state (quartet, HS state).

The magnetic coupling constants extracted from the ab initio procedure are in good agreement with the experimentally extracted values, and the calculated temperature dependence of the effective magnetic moment reproduces well the experimental function, despite the simplicity of the method.

Truhlar's noncollinear procedure applied to the same model system provided an equally accurate HS-LS spin gap, and wave functions that qualitatively reflect the correct physics. Angles among the local spins of the three sites greater than 90° have been obtained, which have been associated to anti-ferromagnetic spin couplings among the three sites for the LS state. However, results on the higher portion of the spin-ladder using the noncollinear approach are not available. It is therefore not possible to extract the magnetic coupling constants predicted by the noncollinear procedure, and make direct comparisons.

Our strategy provides precise details on the spin interactions among the three local spins, that are in perfect agreement with the experimental data available. From a qualitative and quantitative standpoint our strategy is proven robust, and provides a very accurate prediction of the LS-HS spin gap. Moreover, having access to the entire manifold of low-energy states, reliable magnetic coupling constants can be extracted, and a satisfactory effective magnetic moment dependency from the temperature.

Conflicts of interest

There are no conflicts of interest to declare.

Acknowledgments

The author thank Oskar Weser and Nikolay Bogdanov for valuable scientific discussions. The work has been funded by the Max Planck Society.

References

(1) Ghosh, A.; Taylor, P. R. High-level ab initio calculations on the energetics of low-lying spin states of biologically relevant transition metal complexes: a first progress report. *Current Opinion in Chemical Biology* **2003**, *7*, 113 – 124.

(2) Soda, T.; Kitagawa, Y.; Onishi, T.; Takano, Y.; Shigeta, Y.; Nagao, H.; Yoshioka, Y.; Yamaguchi, K. Ab initio computations of effective exchange integrals for H-H,H-He-H and Mn2O2 complex: comparison of broken-symmetry approaches. *Chemical Physics Letters* **2000**, *319*, 223 – 230.

(3) Yamaguchi, K.; Yamanaka, S.; Nishino, M.; Takano, Y.; Kitagawa, Y.; Nagao, H.; Yoshioka, Y. Symmetry and Broken Symmetries in Molecular Orbital Descriptions of Unstable Molecules II. Alignment, Frustration, and Tunneling of Spins in Mesoscopic Molecular Magnets. *Theor. Chem. Acc.* **1999**, *102*, 328–345.

(4) S, Y.; Yamaki, D.; Shigeta, Y.; Nagao, H.; Yamaguchi, K. Noncollinear Spin Density Functional Theory for Spin-Frustratedand Spin-Degenerate Systems. *International Journal of Quantum Chemistry* **2001**, *84*, 670–676.

(5) Löwdin, P.-O.; Mayer, I. Some Studies of the General Hartree–Fock Method. *Advances in Quantum Chemistry* **1992**, *24*, 79–114.

(6) Hammes-Schiffer, S.; Andersen, H. C. The Advantages of the General Hartree–Fock Method for Future Computer Simulation of Materials. *J. Chem. Phys.* **1993**, *99*, 1901–1913.

(7) Luo, S.; Rivalta, I.; Batista, V.; Truhlar, D. G. Noncollinear Spins Provide a Self-Consistent Treatment of the Low-Spin State of a Biomimetic Oxomanganese Synthetic Trimer Inspired by the Oxygen Evolving Complex of Photosystem II. *The Journal of Physical Chemistry Letters* **2011**, *2*, 2629–2633.

(8) Xu, X.; Yang, K. R.; Truhlar, D. G. Testing Noncollinear Spin-Flip, Collinear Spin-Flip, and Conventional Time-Dependent Density Functional Theory for Predicting Electronic Excitation Energies of Closed-Shell Atoms. *Journal of Chemical Theory and Computation* **2014**, *10*, 2070–2084.

(9) Cappelluti, F.; Bencivenni, L.; Guidoni, L. Spin-symmetrised structures and vibrational frequencies of ironâĂŞsulfur clusters. *Phys. Chem. Chem. Phys.* **2020**, *22*, 16655–16664.

(10) Sarneski, J. E.; Thorp, H. H.; Brudvig, G. W.; Crabtree, R. H.; Schulte, G. K. Assembly of high-valent oxomanganese clusters in aqueous solution. Redox equilibrium of water-stable Mn3O44+ and Mn2O23+ complexes. *Journal of the American Chemical Society* **1990**, *112*, 7255–7260.

(11) Krewald, V.; Pantazis, D. A. *Applications of the Density Matrix Renormalization Group to Exchange-Coupled Transition Metal Systems*; Transition Metals in Coordination Environments: Computational Chemistry and Catalysis Viewpoints; Springer International Publishing: Cham, Switzerland, 2019.

(12) Stein, C. J.; Pantazis, D. A.; Krewald, V. Orbital Entanglement Analysis of Exchange-Coupled Systems. *The Journal of Physical Chemistry Letters* **2019**, *10*, 6762–6770.

(13) Paul, S.; Cox, N.; Pantazis, D. A. What Can We Learn from a Biomimetic Model of Nature's Oxygen-Evolving Complex? *Inorganic Chemistry* **2017**, *56*, 3875–3888.

(14) Kurashige, Y.; Chan, G. K.-L.; Yanai, T. Entangled quantum electronic wavefunctions of the Mn_4CaO_5 cluster in photosystem II. *Nat. Chem.* **2013**, *5*, 660–666.

(15) Li, Z.; Guo, S.; Sun, Q.; Chan, G. K.-L. Electronic landscape of the P-cluster of nitrogenase as revealed through many-electron quantum wavefunction simulations. *Nat. Chem.* **2019**, *11*, 1026–1033.

(16) Kawakami, T.; Miyagawa, K.; Sharma, S.; Saito, T.; Shoji, M.; Yamada, S.; Yamanaka, S.; Okumura, M.; Nakajima, T.; Yamaguchi, K. UNO DMRG CAS CI calculations of binuclear manganese complex Mn(IV)2O2(NHCHCO2)4: Scope and applicability of Heisenberg model. *Journal of Computational Chemistry* **2019**, *40*, 333–341.

(17) Sharma, S.; Sivalingam, K.; Neese, F.; Chan, G. K.-L. Low-energy spectrum of iron-sulfur clusters directly from many-particle quantum mechanics. *Nat. Chem.* **2014**, *6*, 927–933.

(18) Li, Z.; Chan, G. K.-L. Spin-Projected Matrix Product States: Versatile Tool for Strongly Correlated Systems. *Journal of Chemical Theory and Computation* **2017**, *13*, 2681–2695.

(19) Booth, G. H.; Thom, A. J. W.; Alavi, A. Fermion Monte Carlo without fixed nodes: A game of life, death, and annihilation in Slater determinant space. *J. Chem. Phys.* **2009**, *131*, 054106.

(20) Cleland, D. M.; Booth, G. H.; Alavi, A. Survival of the Fittest: Accelerating Convergence in Full Configuration-Interaction Quantum Monte Carlo. *J. Chem. Phys.* **2010**, *132*, 041103.

(21) Cleland, D.; Booth, G. H.; Alavi, A. A Study of Electron Affinites Using the Initiator Approach to Full Configuration Interaction Quantum Monte Carlo. *J. Chem. Phys.* **2011**, *134*, 024112.

(22) Overy, C.; Booth, G. H.; Blunt, N. S.; Shepherd, J. J.; Cleland, D.; Alavi, A. Unbiased Reduced Density Matrices and Electronic Properties from Full Configuration Interaction Quantum Monte Carlo. *J. Chem. Phys.* **2014**, *141*, 244117.

(23) Blunt, N. S.; Smart, S. D.; Kersten, J. A.-F.; Spencer, J. S.; Booth, G. H.; Alavi, A. Semi-Stochastic Full Configuration Interaction Quantum Monte Carlo: Developments and Application. *J. Chem. Phys.* **2015**, *142*, 184107.

(24) Booth, G. H.; Smart, S. D.; Alavi, A. Linear-Scaling and Parallelisable Algorithms for Stochastic Quantum Chemistry. *Mol. Phys.* **2014**, *112*, 1855–1869.

(25) Blunt, N. S.; Alavi, A.; Booth, G. H. Krylov-Projected Quantum Monte Carlo Method. *Phys. Rev. Lett.* **2015**, *115*, 050603.

(26) Dobrautz, W.; Smart, S. D.; Alavi, A. Efficient formulation of full configuration interaction quantum Monte Carlo in a spin eigenbasis via the graphical unitary group approach. *J. Chem. Phys.* **2019**, *151*, 094104.

(27) Li Manni, G.; Smart, S. D.; Alavi, A. Combining the Complete Active Space Self-Consistent Field Method and the Full Configuration Interaction Quantum Monte Carlo within a Super-CI Framework, with Application to Challenging Metal-Porphyrins. *J. Chem. Theory Comput.* **2016**, *12*, 1245–1258.

(28) Aquilante, F. et al. Molcas 8: New Capabilities for Multiconfigurational Quantum Chemical Calculations Across the Periodic Table. *J. Comput. Chem.* **2016**, *37*, 506–541.

(29) Fdez. Galván, I. et al. OpenMolcas: From Source Code to Insight. *J. Chem. Theory Comput.* **2019**, *15*, 5925–5964.

(30) Guther, K. et al. NECI: N-Electron Configuration Interaction with an emphasis on state-of-the-art stochastic methods. *The Journal of Chemical Physics* **2020**, *153*, 034107.

(31) Li Manni, G.; Alavi, A. Understanding the Mechanism Stabilizing Intermediate Spin States in Fe(II)-Porphyrin. *J. Phys. Chem. A* **2018**, *122*, 4935–4947.

(32) Bogdanov, N. A.; Li Manni, G.; Sharma, S.; Gunnarsson, O.; Alavi, A. New superexchange paths due to breathing-enhanced hopping in corner-sharing cuprates. *arXiv:1803.07026* **2018**,

(33) Li Manni, G.; Kats, D.; Tew, D. P.; Alavi, A. Role of Valence and Semicore Electron Correlation on Spin Gaps in Fe(II)-Porphyrins. *J. Chem. Theory Comput.* **2019**, *15*, 1492–1497.

(34) Li Manni, G.; Dobrautz, W.; Alavi, A. Compression of Spin-Adapted Multiconfigurational Wave Functions in Exchange-Coupled Polynuclear Spin Systems. *Journal of Chemical Theory and Computation* **2020**, *16*, 2202–2215.

(35) Li Manni, G.; Dobrautz, W.; Bogdanov, A. N.; Guther, K.; Alavi, A. Resolution of Low-Energy States in Spin-Exchange Transition-Metal Clusters: Case Study of Singlet States in $[Fe(III)_4S_4]$ Cubanes. **2020**,

(36) Weser, O.; Freitag, L.; Guther, K.; Alavi, A.; Li Manni, G. Chemical insights into the electronic structure of Fe(II) porphyrin using FCIQMC, DMRG, and generalized active spaces. *International Journal of Quantum Chemistry* **2021**, *121*, e26454.

(37) Paldus, J. Group theoretical approach to the configuration interaction and perturbation theory calculations for atomic and molecular systems. *J. Chem. Phys.* **1974**, *61*, 5321.

(38) Paldus, J. Matrix elements of unitary group generators in many-fermion correlation problem. I. tensorial approaches. *Journal of Mathematical Chemistry* **2020**,

(39) Shavitt, I. Graph theoretical concepts for the unitary group approach to the many-electron correlation problem. *Int. J. Quantum Chem.* **1977**, *12*, 131.

(40) Shavitt, I. Matrix Element Evaluation in the Unitary Group Approach to the Electron Correlation Problem. *Int. J. Quantum Chem.* **1978**, *14 S12*, 5–32.

(41) Garniron, Y.; Scemama, A.; Loos, P.-F.; Caffarel, M. Hybrid stochastic-deterministic calculation of the second-order perturbative contribution of multireference perturbation theory. *The Journal of Chemical Physics* **2017**, *147*, 034101.

(42) Loos, P.-F.; Scemama, A.; Blondel, A.; Garniron, Y.; Caffarel, M.; Jacquemin, D. A Mountaineering Strategy to Excited States: Highly Accurate Reference Energies and Benchmarks. *Journal of Chemical Theory and Computation* **2018**, *14*, 4360–4379.

(43) Garniron, Y.; Scemama, A.; Giner, E.; Caffarel, M.; Loos, P.-F. Selected configuration interaction dressed by perturbation. *The Journal of Chemical Physics* **2018**, *149*, 064103.

(44) Scemama, A.; Benali, A.; Jacquemin, D.; Caffarel, M.; Loos, P.-F. Excitation energies from diffusion Monte Carlo using selected configuration interaction nodes. *The Journal of Chemical Physics* **2018**, *149*, 034108.

(45) Liu, W.; Hoffmann, M. R. iCI: Iterative CI toward full CI. *Journal of Chemical Theory and Computation* **2016**, *12*, 1169–1178.

(46) Liu, W.; Hoffmann, M. R. SDS: the staticâĂŞdynamicâĂŞstatic framework for strongly correlated electrons. *Theor. Chem. Acc.* **2014**, *133*, 1481.

(47) Ma, D.; Li Manni, G.; Gagliardi, L. The generalized active space concept in multiconfigurational self-consistent field methods. *J. Chem. Phys.* **2011**, *135*, 044128.

(48) Ma, D.; Li Manni, G.; Olsen, J.; Gagliardi, L. Second-Order Perturbation Theory for Generalized Active Space Self-Consistent-Field Wave Functions. *J. Chem. Theory Comput.* **2016**, *12*, 3208–3213.

(49) de Graaf, C.; Broer, R. *Magnetic Interactions in Molecules and Solids*; Theoretical Chemistry and Computational Modelling; Springer International Publishing: Cham, 2016.

(50) Sherman, A.; van Vleck, J. H. The Quantum Theory of Valence. *Rev. Mod. Phys.* **1935**, *7*, 167–228.

(51) Widmark, P.-O.; Malmqvist, P.-Å.; Roos, B. O. Density Matrix Averaged Atomic Natural Orbital (ANO) Basis Sets for Correlated Molecular Wave Functions. *Theor. Chem. Acc.* **1990**, *77*, 291–306.

(52) Roos, B. O.; Lindh, R.; Malmqvist, P.-Å.; Veryazov, V.; Widmark, P.-O. Main Group Atoms and Dimers Studied with a New Relativistic ANO Basis Set. *J. Phys. Chem. A* **2004**, *108*, 2851–2858.

(53) Aquilante, F.; Lindh, R.; Pedersen, T. B. Unbiased Auxiliary Basis Sets for Accurate Two-Electron Integral Approximations. *J. Chem. Phys.* **2007**, *127*, 114107.

(54) Aquilante, F.; Pedersen, T. B.; Lindh, R. Low-Cost Evaluation of the Exchange Fock Matrix from Cholesky and Density Fitting Representations of the Electron Repulsion Integrals. *J. Chem. Phys.* **2007**, *126*, 194106.

(55) Aquilante, F.; Pedersen, T. B.; Lindh, R.; Roos, B. O.; de Merás, A. S.; Koch, H. Accurate Ab Initio Density Fitting for Multiconfigurational Self-Consistent Field Methods. *J. Chem. Phys.* **2008**, *129*, 024113.

(56) Aquilante, F.; Gagliardi, L.; Pedersen, T. B.; Lindh, R. Atomic Cholesky Decompo-

sitions: A Route to Unbiased Auxiliary Basis Sets for Density Fitting Approximation with Tunable Accuracy and Efficiency. *J. Chem. Phys.* **2009**, *130*, 154107.

(57) Pedersen, T. B.; Aquilante, F.; Lindh, R. Density Fitting with Auxiliary Basis Sets from Cholesky Decompositions. *Theor. Chem. Acc.* **2009**, *124*, 1–10.

(58) Pipek, J.; Mezey, P. G. A Fast Intrinsic Localization Procedure Applicable for Ab Initio and Semiempirical Linear Combination of Atomic Orbital Wave Functions. *J. Chem. Phys.* **1989**, *90*, 4916–4926.

(59) Kambe, K. On the Paramagnetic Susceptibilities of Some Polynuclear Complex Salts. *J. Phys. Soc. Jpn.* **1950**, *5*, 48–51.

(60) Boča, R. *Theoretical Foundations of Molecular Magnetism, Volume 1*; Current Methods in Inorganic Chemistry; Elsevier, 1999; pp 724–752.

(61) Hoppe, J. I. Effective magnetic moment. *Journal of Chemical Education* **1972**, *49*, 505.

(62) Anderson, P. W.; Hasegawa, H. Considerations on Double Exchange. *Phys. Rev.* **1955**, *100*, 675–681.

(63) Noodleman, L.; Peng, C.; Case, D.; Mouesca, J.-M. Orbital interactions, electron delocalization and spin coupling in iron-sulfur clusters. *Coord. Chem. Rev.* **1995**, *144*, 199 – 244.

(64) Girerd, J. Electron transfer between magnetic ions in mixed valence binuclear systems. *J. Chem. Phys.* **1983**, *79*, 1766–1775.

Table 1: Leading CSFs of the two doublet and four quartet states within the CASSCF(9,9). Values in parenthesis refer to the weights within the larger active space, CAS(53,37). Symbols u and d refers to the cumulative up (**u**) and down (**d**) spin couplings, respectively.

Mn_A	Mn_B	Mn_C	Weight [%]
$\|LS\rangle = \|S_{AB}, S_{total}\rangle = \|1, 1/2\rangle$			
uuu	ddu	ddu	37.1 (27.1)
uuu	ddu	dud	12.2 (8.8)
uuu	ddu	udd	6.1 (4.5)
uuu	dud	ddu	18.5 (13.8)
uuu	dud	dud	6.1 (4.5)
uuu	dud	udd	3.0 (2.2)
uuu	udd	ddu	10.9 (8.0)
uuu	udd	dud	3.6 (2.6)
uuu	udd	udd	1.8 (1.3)
$\|S_{AB}, S_{total}\rangle = \|2, 1/2\rangle$			
uuu	duu	ddd	50.0
uuu	udu	ddd	29.8
uuu	uud	ddd	19.5
$\|HS\rangle = \|S_{AB}, S_{total}\rangle = \|0, 3/2\rangle$			
uuu	ddd	uuu	99.5 (76.7)
$\|S_{AB}, S_{total}\rangle = \|1, 3/2\rangle$			
uuu	ddu	duu	30.7
uuu	ddu	udu	15.3
uuu	ddu	uud	09.0
uuu	dud	duu	15.6
uuu	dud	udu	07.8
uuu	dud	uud	04.6
uuu	udd	duu	09.2
uuu	udd	udu	04.6
uuu	udd	uud	02.7
$\|S_{AB}, S_{total}\rangle = \|2, 3/2\rangle$			
uuu	duu	ddu	25.2
uuu	duu	dud	14.9
uuu	duu	udd	9.9
uuu	udu	ddu	14.9
uuu	udu	dud	8.7
uuu	udu	udd	5.8
uuu	uud	ddu	10.2
uuu	uud	dud	6.0
uuu	uud	udd	4.0
$\|S_{AB}, S_{total}\rangle = \|3, 3/2\rangle$			
uuu	uuu	ddd	99.6